

Wave Characteristics of Multi-Walled Carbon Nanotubes

Mira Mitra¹ and S. Gopalakrishnan²

Abstract: In this paper, the wave characteristics, namely, the spectrum and dispersion relations of multi-wall carbon nanotubes (MWNTs) are studied. The MWNTs are modeled as multiple thin shells coupled through van der Waals force. Each wall of the MWNT has three displacements, *i.e.*, axial, circumferential and radial with variation along the axial and circumferential directions. The wave characteristics are obtained by transforming the governing differential wave equations to frequency domain via Fourier transform. This transformation is first done in time using fast Fourier transform (FFT) and then in one spatial dimension using Fourier series. These transformed equations are solved by posing them as polynomial eigenvalue problem (PEP). The solution gives the wavenumbers and the wave speeds. First, the wave properties are studied for infinite length MWNT which does not have any variation along the axial direction. Next, the wavenumbers are studied for finite length MWNT with small and large radii. The analysis is done for single, double and three-walled carbon nanotubes.

Keyword: Carbon nanotubes; wave propagation; wavenumbers; wave speeds.

1 Introduction

The recent trend of research in the area of carbon nanotubes (CNTs) shows a growing interest in studying their vibrational and wave characteristics. The understanding of the dynamical properties of CNTs is essential for applications

like sensors, high frequency oscillators and several other nano-devices [Dresselhaus and Eklund (2000), Jiang, Lu, Yu, and Huang (2008)]. Though an extensive experimental research is ongoing to understand the behavior of CNTs, a parallel effort is being given to develop high fidelity theoretical models of CNTs and their devices. The atomistic simulation, though very realistic and accurate, has restricted use for the large computational cost involved. This is more prominent for device applications of CNTs, where they are used in conjunction with host materials and there is a scale difference between the CNT and the host [Srivastava, Wei, and Cho (2003)]. Continuum modeling of CNTs based on different beam and shell theories is found to give appreciable comparison with experimental and atomistic simulation results. There are also hybrid atomistic-continuum modeling which are recently being explored by researchers [Theodosiou and Saravanos (2007); Park, Cho, Kim, Jun, and Im (2006)]

Vibration and wave propagation in multi-walled carbon nanotubes (MWNTs) have been studied by modeling them as Euler-Bernoulli beam [Yoon, Ru, and Mioduchowski (2003b,a)] and later the model has been extended to Timoshenko [Yoon, Ru, and Mioduchowski (2004)] beam theory. The wave properties of MWNTs modeled as multiple Euler-Bernoulli beam with non-coaxial deformation has been studied by Chakraborty and Gopalakrishnan (2006). Nano-composite beam with MWNT embedded in different matrix materials is modeled using higher order layer-wise beam theory [Mitra and Gopalakrishnan (2006)]. The model incorporated partial stress transfer between the MWNT and the matrix. The vibration properties of MWNT were also studied by implementing micropolar mechanics [Xie and Long (2006)]. Continuum 3-D elasto-dynamic equations have also been considered to study the vi-

¹ Department of Aerospace Engineering, Indian Institute of Technology, Bombay, Mumbai 400 076. INDIA, e-mail: mira@aero.iitb.ac.in

² Department of Aerospace Engineering, Indian Institute of Science, Bangalore 560 012. INDIA, e-mail: krishnan@aero.iisc.ernet.in, Fax: +91-80-2360-0134

bration and wave characteristics of mainly single-walled carbon nanotubes (SWNTs) [Mitra and Gopalakrishnan (2007); Chico and Pérez-Álvarez (2004); Suzuura and Ando (2002); Raichura, Dutta, and Stroschio (2003)]. MWNTs have been commonly modeled as multiple shell coupled through van der Waals force using shell theory. The wave characteristics of MWNTs are studied by modeling them as multiple elastic cylindrical structures [Xie, Han, and Long (2007)]. In reference [Wang, Ru, and Mioduchowski (2004b)], the viability of using shell theory for buckling and free vibration analysis of SWNT and MWNT is discussed. Vibrational characteristics of MWNT are studied using Flügge's equation in reference [Wang, Ru, and Mioduchowski (2005a,b)]. Natsuki, Endo, and Tsuda (2006, 2007) used Flügge's equation to study wave propagation in embedded single and double-walled CNTs and also fluid-filled CNT. Vibrational properties of MWNTs are also studied using Donnell shell theory [Sun and Liu (2007)]. However, these references except [Natsuki, Endo, and Tsuda (2007)] are restricted to the study of fundamental natural frequencies. In the reference [Natsuki, Endo, and Tsuda (2007)], the dispersion relations were obtained, but only for double-walled carbon nanotube. The present paper aims on obtaining the wave properties namely, spectrum and dispersion relations, *i.e.*, the wavenumbers and wave speeds of MWNT with different configurations. The mathematical technique implemented in the present work can be used to obtain the wave characteristics of MWNT with arbitrary number of walls coupled through van der Waals forces. The study of these wave properties brings out several new wave characteristics that are not observed in conventional structures. It is essential to properly understand these properties prior to using CNTs for nano-scale devices and also to explore new applications of CNTs.

Here, the MWNT is modeled as multiple thin shell coupled through inter-wall van der Waals forces using Flügge's shell theory. Each wall has axial, circumferential and radial degrees of freedom with variation along axial and circumferential directions. The governing equations

are first reduced to frequency domain through Fourier transform in time. The Fourier transform is implemented through fast Fourier transform (FFT). Next, a Fourier series approximation is performed in the axial/circumferential direction, to further reduce the equations to ordinary differential equations (ODEs) in the frequency-wavenumber domain. These ODEs have constant coefficients and are solve by posing them as polynomial eigenvalue problem (PEP). This method has been implemented to study wave propagation in laminated composite plate [Chakraborty and Gopalakrishnan (2005)]. The solution of the PEP provides the wavenumbers and wave amplitude as a function of the frequency and axial/circumferential wavenumber, depending on the direction along which the Fourier series approximation is performed. The main advantage of the technique is that it is fully automated and can solve complicated structures. The study is performed, first, for infinite length MWNT without any variation of the displacements along axial direction. For this case, the axial mode is uncoupled, while the radial and circumferential modes are coupled. Next, the example of finite length MWNT with variation along both axial and circumferential directions are studied. Here, all the three modes are coupled.

The paper is organized as follows. In the next section there are three subsections on the governing differential equations, reduction of the equations through Fourier transform and calculation of wavenumbers and wave speeds, respectively. Section 3 presents the numerical experiments performed. The examples are presented for single, double and three-walled carbon nanotubes. However, the technique can be implemented for any arbitrary number of walls. The wavenumbers and wave speeds are obtained for different values of axial/circumferential wavenumbers for MWNTs of different radii. The paper ends with important conclusions.

2 Mathematical Formulation

2.1 Governing Differential Equations

As mentioned earlier, the wave characteristics of MWNT are studied by modeling them as multiple thin shell using Flügge's equation [Markus (1988)]. These equations for MWNTs are much simplified due to the absence of prestresses [Wang, Ru, and Mioduchowski (2004b)]. The set of equations for each wall is coupled to the adjacent walls through inter-wall van der Waals forces. The equations for the p^{th} wall are given as

$$\begin{aligned} & \frac{\partial^2 u_p}{\partial x^2} + \frac{(1-\nu)}{2R_p^2} \frac{\partial^2 u_p}{\partial \theta^2} + \frac{(1+\nu)}{2R_p} \frac{\partial^2 v_p}{\partial x \partial \theta} + \frac{\nu}{R} \frac{\partial w}{\partial x} \\ & + \frac{(1-\nu^2)D}{EhR_p^2} \\ & \cdot \left[\frac{(1-\nu)}{2R_p^2} \frac{\partial^2 u_p}{\partial \theta^2} - R_p \frac{\partial^3 w_p}{\partial x^3} + \frac{(1-\nu)}{2R_p} \frac{\partial^3 w_p}{\partial x \partial^2 \theta} \right] \\ & = \frac{\rho h(1-\nu^2)}{Eh} \frac{\partial^2 u_p}{\partial t^2} \quad (1) \end{aligned}$$

$$\begin{aligned} & \frac{(1+\nu)}{2R_p} \frac{\partial^2 u_p}{\partial x \partial \theta} + \frac{(1+\nu)}{2} \frac{\partial v_p}{\partial x^2} \\ & + \frac{1}{R_p^2} \frac{\partial^2 v_p}{\partial \theta^2} + \frac{1}{R_p^2} \frac{\partial w_p}{\partial \theta} \\ & + \frac{(1-\nu^2)D}{EhR_p^2} \left[\frac{3(1-\nu)}{2} \frac{\partial^2 v_p}{\partial x^2} - \frac{(3-\nu)}{2} \frac{\partial^3 w_p}{\partial x^2 \partial \theta} \right] \\ & = \frac{\rho h(1-\nu^2)}{Eh} \frac{\partial^2 v_p}{\partial t^2} \quad (2) \end{aligned}$$

$$\begin{aligned} & \frac{\nu}{R_p} \frac{\partial u_p}{\partial x} + \frac{1}{R_p^2} \frac{\partial v_p}{\partial \theta} - \frac{1}{R_p^2} w_p \\ & + \frac{(1-\nu^2)D}{EhR_p^2} \left[R_p^2 \frac{\partial^4 w_p}{\partial x^4} + 2 \frac{\partial^4 w_p}{\partial x^2 \partial \theta^2} + \frac{1}{R_p^2} \frac{\partial^4 w_p}{\partial \theta^4} \right. \\ & - R_p \frac{\partial^3 u_p}{\partial x^3} + \frac{(1-\nu)}{2R_p} \frac{\partial^3 u_p}{\partial x \partial \theta^2} - \frac{(3-\nu)}{2} \frac{\partial^3 v_p}{\partial x^2 \partial \theta} \\ & \left. - \frac{1}{R_p^2} w_p - \frac{2}{R_p^2} \frac{\partial^2 w_p}{\partial \theta^2} \right] \\ & = \frac{\rho h(1-\nu^2)}{Eh} \frac{\partial^2 w_p}{\partial t^2} - P_p \quad (3) \end{aligned}$$

where, u_p , v_p and w_p are the axial, circumferential and radial displacements of the p^{th} wall respectively. These displacements are function of x , θ and t . R_p is the centerline radius of the p^{th} and h is the thickness of each wall, also the inter-wall distance. E , ρ , ν and D are the Young's modulus, mass density, Poisson's ratio and the effective bending stiffness respectively. The numerical values of these parameters are explained in Section 3 on numerical experiments.

The inter-wall van der Waals force denoted as P_p for the p^{th} wall in Eqn. 3 has the following form [Wang, Ru, and Mioduchowski (2005a)],

$$P_p = c(w_{p+1} - w_p) - c \frac{R_{p-1}}{R_p} (w_p - w_{p-1})$$

for $p = 2, 3, \dots, P-1$ (4)

and for $p = 1$ and $p = P$, it is given as,

$$P_1 = c(w_2 - w_1) \quad \text{and} \quad P_P = -c \frac{R_{P-1}}{R_P} (w_P - w_{P-1}) \quad (5)$$

The value of the van der Waals interaction coefficient c is given as [Wang, Ru, and Mioduchowski (2005a)],

$$c = \frac{320 \times \text{erg/cm}^2}{0.16d^2} \quad \text{where, } d = 0.142 \text{ nm} \quad (6)$$

Thus, the governing equations for one wall are coupled to that of the others through the inter-wall van der Waals interaction given by P_p for the p^{th} wall as shown in Eqn. 3.

In this paper, the wave characteristics are presented first for an infinite length MWNT. To simulate this condition, the variation along the axial, (x) direction is neglected. This assumption makes the Eqn. 1 for axial displacement uncoupled to the other two Eqns. 2 and 3. Next, the wave characteristics are obtained considering variation along both axial, (x) and circumferential (θ) directions. In the next subsection, the governing equations (Eqns. 1 to 3) are reduced to ODEs through FFT and Fourier series transformation in time and axial directions respectively. The reduced ODEs are solved by posing them as PEP.

2.2 Calculation of Wavenumbers

The displacements u_p , v_p and w_p for an arbitrary wall p is approximated using FFT is time and Fourier series in axial, x direction as given below,

$$u_p(x, \theta, t) = \sum_{n=0}^{N-1} \sum_{m=0}^{M-1} \hat{u}_p(\theta) \cos(\xi_m x) e^{-j\omega_n t} \quad (7)$$

$$v_p(x, \theta, t) = \sum_{n=0}^{N-1} \sum_{m=0}^{M-1} \hat{v}_p(\theta) \sin(\xi_m x) e^{-j\omega_n t} \quad (8)$$

$$w_p(x, \theta, t) = \sum_{n=0}^{N-1} \sum_{m=0}^{M-1} \hat{w}_p(\theta) \sin(\xi_m x) e^{-j\omega_n t} \quad (9)$$

where, N and M are the number of time sampling points and number spatial sampling points respectively. ω_n is the circular frequency at the n^{th} time sample. Similarly, ξ_m is the axial wavenumber at the m^{th} spatial sample point. Substituting Eqns. 7 to 9 into the governing wave equations (Eqns. 1 to 3), we get the reduced equations as follows. Hereafter the subscripts n and m in Eqns. 7 to 9 are dropped for simplified notations.

$$\begin{aligned} & -\xi^2 \hat{u}_p + \frac{(1-\nu)}{2R_p^2} \frac{d^2 \hat{u}_p}{d\theta^2} + \frac{(1+\nu)\xi}{2R_p} \frac{d\hat{v}_p}{d\theta} + \frac{\nu}{R_p} \xi \hat{w}_p \\ & + \frac{(1-\nu^2)D}{EhR_p^2} \\ & \cdot \left[\frac{(1-\nu)}{2R_p^2} \frac{d^2 \hat{u}_p}{d\theta^2} + R_p \xi^3 \hat{w}_p - \frac{(1-\nu)\xi}{2R_p} \frac{d^2 \hat{w}_p}{d\theta^2} \right] \\ & = -\omega^2 \frac{\rho h(1-\nu^2)}{Eh} \hat{u}_p \quad (10) \end{aligned}$$

$$\begin{aligned} & -\frac{(1+\nu)}{2R_p} \xi \frac{d\hat{u}_p}{d\theta} - \frac{(1+\nu)}{2} \xi^2 \hat{v}_p \\ & + \frac{1}{R_p^2} \frac{d^2 \hat{v}_p}{d\theta^2} + \frac{1}{R_p^2} \frac{d\hat{w}_p}{d\theta} \\ & + \frac{(1-\nu^2)D}{EhR_p^2} \left[-\frac{3(1-\nu)}{2} \xi^2 \hat{v}_p + \frac{(3-\nu)}{2} \xi^2 \frac{d\hat{w}_p}{d\theta} \right] \\ & = -\omega^2 \frac{\rho h(1-\nu^2)}{Eh} \hat{v}_p \quad (11) \end{aligned}$$

$$\begin{aligned} & -\frac{\nu}{R_p} \xi \hat{u}_p + \frac{1}{R_p^2} \frac{d\hat{v}_p}{d\theta} - \frac{1}{R_p^2} \hat{w}_p \\ & + \frac{(1-\nu^2)D}{EhR_p^2} \left[R_p^2 \xi^4 \hat{w}_p - 2\xi^2 \frac{d^2 \hat{w}_p}{d\theta^2} + \frac{1}{R_p^2} \frac{d^4 \hat{w}_p}{d\theta^4} \right. \\ & \left. - R_p \xi^3 \hat{u}_p - \frac{(1-\nu)\xi}{2R_p} \frac{d^2 \hat{u}_p}{d\theta^2} + \frac{(3-\nu)}{2} \xi^2 \frac{d^2 \hat{w}_p}{d\theta^2} \right] \\ & = -\omega^2 \frac{\rho h(1-\nu^2)}{Eh} \hat{w}_p + \frac{(1-\nu^2)}{Eh} \left[c(\hat{w}_{p+1} - \hat{w}_p) \right. \\ & \left. - c \frac{R_{p-1}}{R_p} (\hat{w}_p - \hat{w}_{p-1}) \right] \quad (12) \end{aligned}$$

The above ODEs are required to be solve for the transformed displacements \hat{u}_p , \hat{v}_p and \hat{w}_p . For these constant coefficient equations, the solutions are of the following form,

$$\hat{u}_p(\theta) = \sum \tilde{u}_p e^{-jk\theta} \quad (13)$$

$$\hat{v}_p(\theta) = \sum \tilde{v}_p e^{-jk\theta} \quad (14)$$

$$\hat{w}_p(\theta) = \sum \tilde{w}_p e^{-jk\theta} \quad (15)$$

Substituting Eqns. 13 to 15 in Eqns. 10 to 12, neglecting the coupling term and writing it in matrix form, we get the PEP as,

$$\mathbf{A}_p^0 k^4 + \mathbf{A}_p^1 k^3 + \mathbf{A}_p^2 k^2 + \mathbf{A}_p^3 k + \mathbf{A}_p^4 = 0 \quad (16)$$

where,

$$\mathbf{A}_p^0 = \begin{bmatrix} 0 & 0 & 0 \\ 0 & 0 & 0 \\ 0 & 0 & \frac{\alpha}{R_p^2} \end{bmatrix} \quad \mathbf{A}_p^1 = \begin{bmatrix} 0 & 0 & 0 \\ 0 & 0 & 0 \\ 0 & 0 & 0 \end{bmatrix}$$

$$\mathbf{A}_p^2 = \begin{bmatrix} -\frac{(1+\alpha)(1-\nu)}{2R_p} & 0 & \frac{j\alpha\xi(1-\nu)}{2R_p} \\ 0 & -1 & 0 \\ \frac{j\alpha\xi(1-\nu)}{2R_p} & 0 & 2\alpha\xi^2 - 2\frac{\alpha}{R_p^2} \end{bmatrix}$$

$$\mathbf{A}_p^3 = \begin{bmatrix} 0 & -\frac{\xi(1+\nu)}{2R_p} & 0 \\ -\frac{\xi(1+\nu)}{2R_p} & 0 & -\frac{j\alpha\xi^2(3-\nu)}{2} - j \\ 0 & -\frac{j\alpha\xi^2(3-\nu)}{2} - j & 0 \end{bmatrix}$$

$$\mathbf{A}_p^4 = \begin{bmatrix} -\xi^2 + \omega^2 \kappa & 0 \\ 0 & -\frac{\xi^2(3\alpha+1)(1-\nu)}{2} + \omega^2 \kappa \\ -j\alpha\xi^3 R_p - \frac{j\xi\nu}{R_p} & 0 \\ -j\alpha\xi^3 R_p - \frac{j\xi\nu}{R_p} & \\ 0 & \\ \alpha\xi^4 R_p^2 - j\alpha\xi^3 R_p + (1-\alpha) - \omega^2 \kappa & \end{bmatrix}$$

where, $\alpha = \frac{(1-\nu^2)D}{EhR_p^2}$ and $\kappa = \frac{\rho h(1-\nu^2)}{Eh}$. Next, the PEP for the coupled P -walled MWNT is obtained as,

$$\mathbf{A}^0 k^4 + \mathbf{A}^1 k^3 + \mathbf{A}^2 k^2 + \mathbf{A}^3 k + \mathbf{A}^4 = 0 \quad (17)$$

where, the dimensions of \mathbf{A}^0 to \mathbf{A}^4 is $3P \times 3P$ and the matrix \mathbf{A}^i , $i = 1$ to 4 is of the form

$$\mathbf{A}^i = \begin{bmatrix} \dots & \vdots & \vdots & \vdots & \dots \\ \dots & \mathbf{A}_{p-1}^i & 0 & 0 & \dots \\ \dots & 0 & \mathbf{A}_p^i & 0 & \dots \\ \dots & 0 & 0 & \mathbf{A}_{p+1}^i & \dots \\ \dots & \vdots & \vdots & \vdots & \dots \end{bmatrix}$$

For the coupled system, the matrix \mathbf{A}^4 is obtained as,

$$\mathbf{A}^4 = \begin{bmatrix} \dots & \vdots & \vdots & \vdots & \dots \\ \dots & \mathbf{A}_{p-1}^4 & 0 & 0 & \dots \\ \dots & 0 & \mathbf{A}_p^4 & 0 & \dots \\ \dots & 0 & 0 & \mathbf{A}_{p+1}^4 & \dots \\ \dots & \vdots & \vdots & \vdots & \dots \end{bmatrix} + [C]$$

where, $[C]$ is the coupling matrix obtained from Eqn. 4 and is of dimension $3P \times 3P$. The matrix

has the following form,

$$[C] = \begin{bmatrix} \dots & \vdots & \vdots \\ \dots & -c\beta \frac{R_{p-2}}{R_{p-1}} & c\beta \left(1 + \frac{R_{p-2}}{R_{p-1}}\right) \\ \dots & 0 & -c\beta \frac{R_{p-1}}{R_p} \\ \dots & 0 & 0 \\ \dots & \vdots & \vdots \\ \vdots & \vdots & \vdots & \dots \\ -c\beta & 0 & 0 & \dots \\ c\beta \left(1 + \frac{R_{p-1}}{R_p}\right) & -c\beta & 0 & \dots \\ -c\beta \frac{R_p}{R_{p+1}} & c\beta \left(1 + \frac{R_p}{R_{p+1}}\right) & -c\beta & \dots \\ \vdots & \vdots & \vdots & \dots \end{bmatrix} \quad (18)$$

where, $\beta = \frac{(1-\nu^2)}{Eh}$. The above PEP given by Eqn. 17 is very generalized and can be solved easily for MWNT with arbitrary number of walls. The solution is done for the wavenumbers in circumferential direction k . As said earlier, these wavenumbers are function of frequency ω and axial wavenumber ξ . The corresponding phase speed is calculated as $C_p = \text{real}\left(\frac{\omega}{k}\right)$. Similarly, the group speed is derived as $C_g = \text{real}\left(\frac{d\omega}{dk}\right)$. It should be mentioned here that, to obtain the wavenumbers in axial direction, the Fourier series transform should be performed in the circumferential direction.

3 Numerical Experiments

In this section, numerical experiments are presented to analyze the wave properties of MWNTs. First, the wavenumber, phase and group speeds are obtained for MWNT of infinite length, *i.e.*, the displacements do not have variation along axial direction. Next, the radial wavenumbers of a MWNT for given axial wavenumbers are studied. These examples are presented for different values of the innermost radius. Finally, the axial wavenumbers are studied for a given radial wavenumber. All the above results are presented for single, double and three-walled carbon nanotubes. However, as said earlier, the analysis tech-

nique can be easily applied for any arbitrary number of walls.

The bulk material properties of each wall of the MWNT are as follows, Young's modulus, $Eh = 360 \text{ J/m}^2$ [Yakobsen, Brabec, and Bernholc (1996)], mass density, $\rho h = 2.27 \times 0.34 \text{ kg/m}^3$ and Poisson's ratio, $\nu = 0.2$ [Wang, Ru, and Mioduchowski (2004a)]. In particular, these parameters are dependent on the definition of wall thickness $2h$ [Yakobsen, Brabec, and Bernholc (1996)]. The effective bending stiffness, D is taken as $D = 2 \text{ eV}$, as suggested by Saito, Takeya, Kimura, Dresselhaus, and Dresselhaus (1998). This value of D gives a better comparison between the atomistic simulation and the continuum model simulation. The conversion factor from eV to Nm^2 is 1.6021×10^{-19} . The distance between the walls of the MWNT is taken as 0.34 nm .

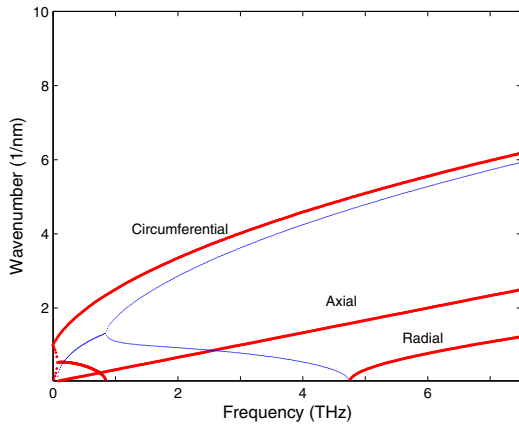
Figs. 1(a), (b) and (c) show the real and imaginary parts of the circumferential wavenumber of single, double and three-walled carbon nanotubes respectively. These wavenumbers are obtained assuming variation only in the circumferential direction. The thick lines represent the real part and the thin lines show the imaginary part of the wavenumbers. The innermost radius in all the cases is considered as $R = 0.678 \text{ nm}$. From Fig. 1(a), for single walled carbon nanotube (SWNT), it can be seen that there are three modes of wave propagation, namely, axial, circumferential and radial. The wavenumbers for the axial mode has a linear variation with the frequency which is in the THz range. The linear variation of the wavenumbers denote that the waves will propagate non-dispersively, i.e, the waves do not change their shapes as they propagate. On the other hand, the circumferential wavenumbers have a non-linear variation with the frequency, which indicates that the waves are dispersive in nature. However, the wavenumbers of this circumferential wave mode have a substantial real part starting from the zero frequency. This implies that the mode starts propagating at any excitation frequency and does not have a cut-off frequency. The radial mode, however, has a certain frequency band within which the corresponding wavenumbers are purely imaginary. Thus, the ra-

dial mode does not propagate at frequencies lying within this band. Both the circumferential and radial wavenumbers have a substantial imaginary part along with the real part, thus these waves attenuate as they propagate.

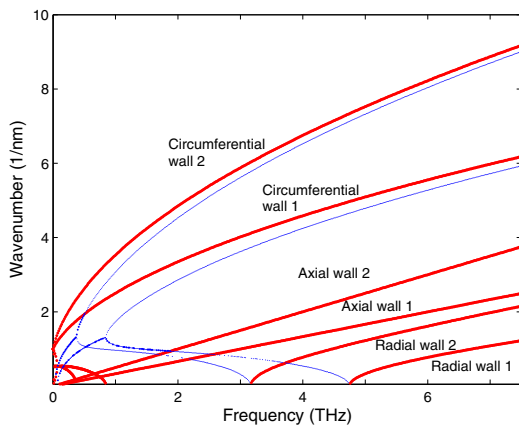
Similar observations can be done from Fig. 1(b), where the wavenumbers are plotted for a double walled carbon nanotube. Here, there are six modes, three corresponding to each wall. The wavenumbers for the outer wall are higher than that for the inner wall, for all the three modes. In Fig. 1(c), the wavenumbers are presented for a three-walled carbon nanotube. As expected, here there are nine modes, three corresponding to each of the three walls. It should be mentioned that these wave characteristics are not effected significantly by the van der Waals interaction between the walls.

Fig. 2(a), plots the phase speeds for the three-walled carbon nanotube used in the previous example. The phase speed for the axial mode has a constant value for all the frequencies and hence, the wave does not change its shape as it propagates. It can also be observed, that the axial phase speed is nearly similar for all the three walls. This is because the variation of the axial phase speed with the radius of the nanotube wall is not significant. Similarly, the circumferential phase speeds for the three walls also do not defer much. In tune with that observed from the wavenumber plots shown in Fig. 1(c), the phase speed for the radial mode does not exist between a frequency band. The range of this band shifts for different walls of the MWNT. In Fig. 2(b), the corresponding group speeds are presented. For the group speeds, except the axial mode, the difference in the values for different walls of the MWNT is quite significant unlike the phase speed and the speed of the outer wall is higher than that of the inner wall.

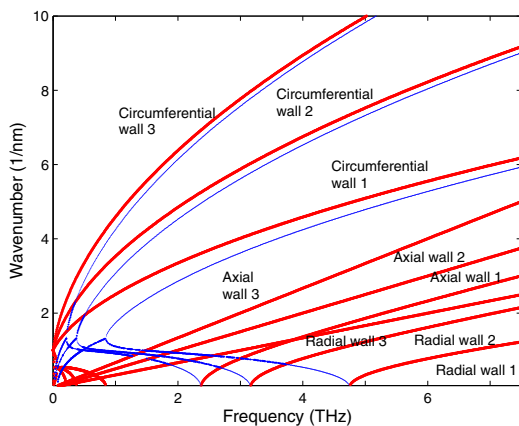
In Figs. 3(a) to (c), the variation of circumferential wavenumbers are plotted for single, double and three-walled carbon nanotubes respectively, with innermost radius of 0.678 nm . These wavenumbers are plotted for an axial wavenumber of $K_z R = 1$. Here, a finite length MWNT is considered and for such case a coupling exists between the axial, circumferential and radial wave modes. In



(a)

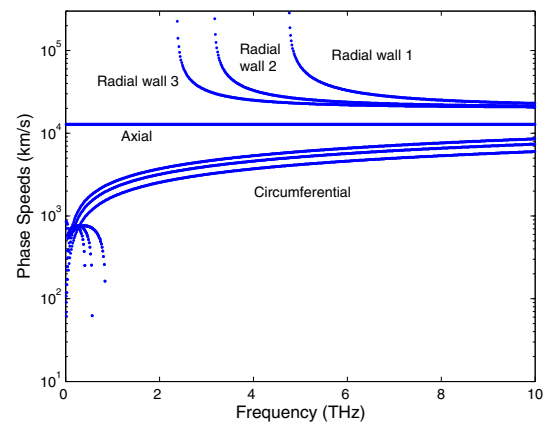


(b)

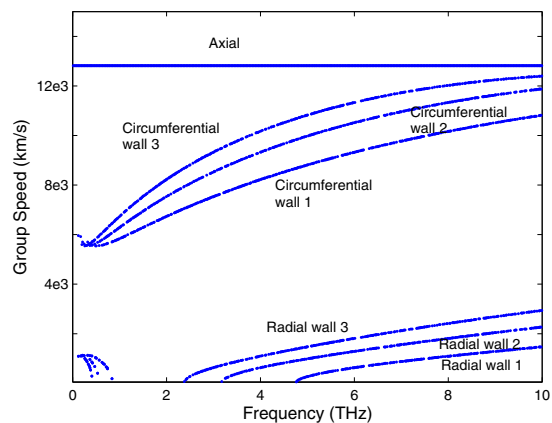


(c)

Figure 1: Real (thick line) and imaginary (thin line) parts of the wavenumbers of (a) single, (b) double and (c) three walled carbon nanotubes.



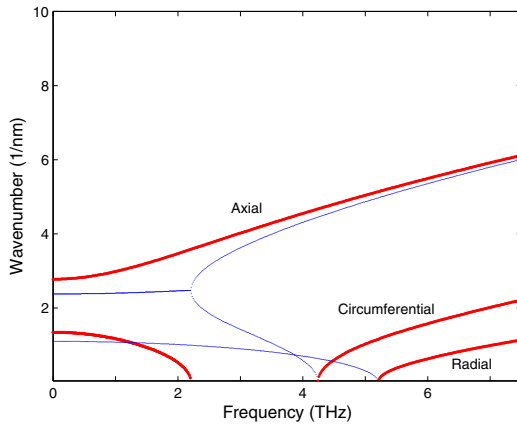
(a)



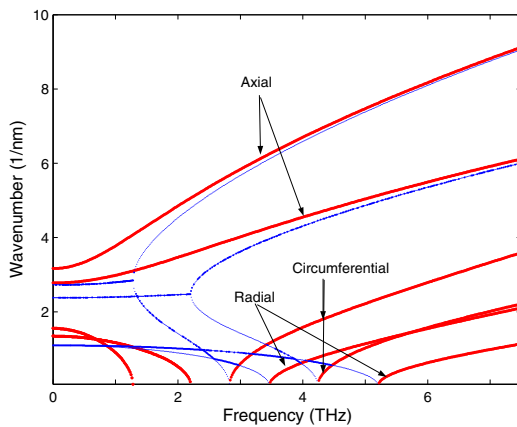
(b)

Figure 2: (a) Phase and (b) group speeds of a three walled carbon nanotube

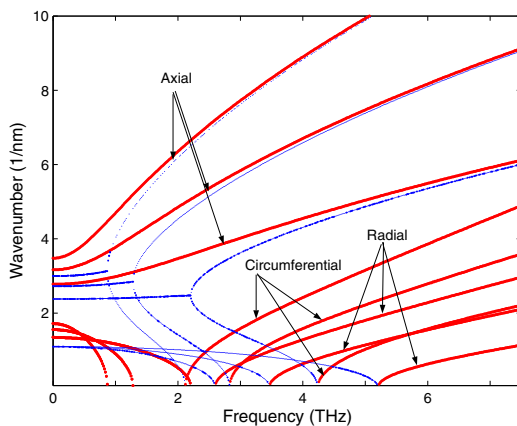
Fig. 3(a), it can be seen that the axial mode has a non-linear variation with frequency unlike that for an infinite MWNT shown in Fig. 1(a). This non-linear variation occur due to the coupling arising from the finiteness of the MWNT. Thus, here, the axial modes are dispersive in nature. Next, the real part of the wavenumbers for the circumferential mode exists after a certain frequency referred as the cut-off frequency. This implies that the mode start propagating only after the cut-off frequency. This behavior is also not in tune with that observed for infinite MWNT in Figs. 1, where such cut-off frequency does not exist for the circumferential mode. The radial mode, however, shows similar pattern as in Fig. 1 and has a frequency band within which the waves do not prop-



(a)



(b)



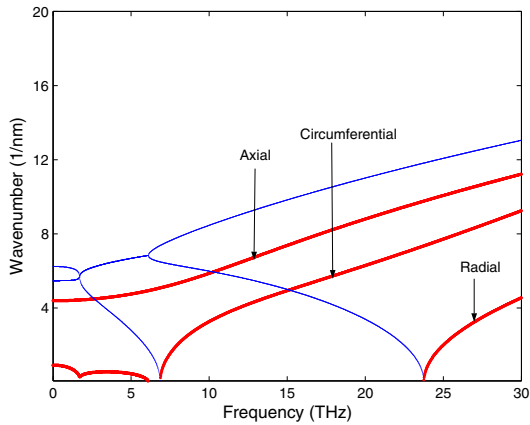
(c)

Figure 3: Real (thick line) and imaginary (thin line) parts of the wavenumbers of (a) single, (b) double and (c) three walled carbon nanotubes at axial wavenumber $k_z R = 1$.

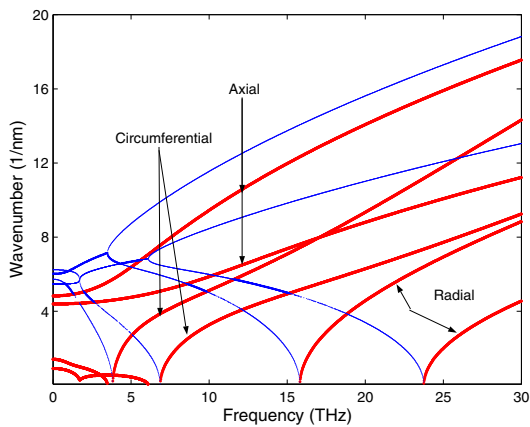
agate. In addition to this real part of the wavenumbers, there is a substantial imaginary part shown as thin lines in the plot. This imaginary part attenuates the waves as they propagate. In Figs. 3(b) and (c), similar wavenumber plots are presented for double and three-walled carbon nanotubes. The plots show similar trend and the wavenumbers are higher for the outer walls for all the three modes. The cut-off frequencies for the circumferential modes also decrease for the outer walls.

Figs. 4(a) to (c), show the wavenumber plot similar to that presented in the previous example (Fig. 3), except that the axial wavenumber here is $K_z R = 5$. It can be seen, that the change in the axial wavenumber results in substantial change in the pattern and the amplitude of the wavenumbers. The dimensions of the MWNT are kept same as before, *i.e.*, the innermost diameter is 0.678 nm and the inter-wall spacing is 0.34 nm. In addition to the increase in amplitude as compared to the Fig. 3, the cut-off frequency band of the radial wave mode has also increased considerably, while the cut-off frequency of the circumferential mode has increased slightly (≈ 1 THz).

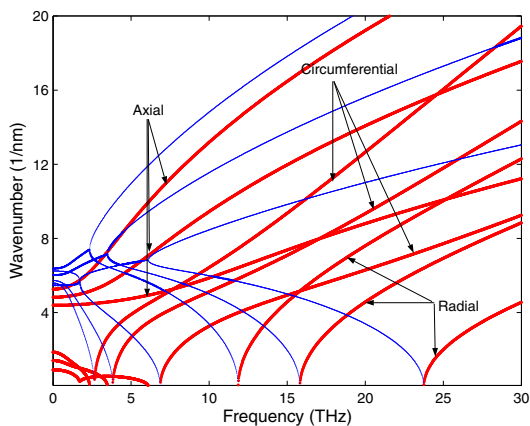
Next, the wavenumbers are obtained for three-walled carbon nanotubes with different radii of the innermost wall. The three different radii considered are 1.0, 2.0 and 5.0 nm and the corresponding wavenumbers are plotted in Figs. 5(a), (b) and (c) respectively. The axial wavenumber is $k_z R = 1$ and the inter-wall spacing is 0.34 nm. With the increase in the radius of the innermost wall of the nanotube, the amplitude of the wavenumbers increases for all the three modes. The cut-off frequencies for the circumferential modes also decreases with increase in the radius. The most substantial difference is observed in the cut-off frequency band for the radial mode, which reduces from ≈ 2.0 THz for $R = 1.0$ nm to almost zero for $R = 5.0$ nm. The main conclusion that can be drawn from this numerical experiment is that for higher values of the radius of the innermost wall of the MWNT, the wavenumber plots for the different walls nearly coincides. Thus, for a MWNT with radius than a certain value can be modeled as equivalent single-walled nanotube (SWNT) for wave prop-



(a)



(b)



(c)

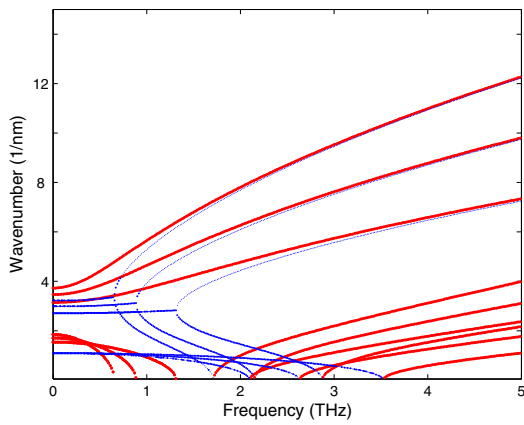
Figure 4: Real (thick line) and imaginary (thin line) parts of the wavenumbers of (a) single, (b) double and (c) three walled carbon nanotubes at axial wavenumber $k_z R = 5$.

agation analysis. This will reduce the complexities of modeling a MWNT. It should be mentioned here that the above observation is in tune with that observed with Euler-Bernoulli beam model of MWNT studied by Chakraborty, Sivakumar, and Gopalakrishnan (2006). The spectrum relation of MWNT modeled as multiple Euler-Bernoulli beam coupled through van der Waals force are presented by Chakraborty, Sivakumar, and Gopalakrishnan (2006). For such case also, the wavenumber plots nearly coincide for the outer walls of the MWNT.

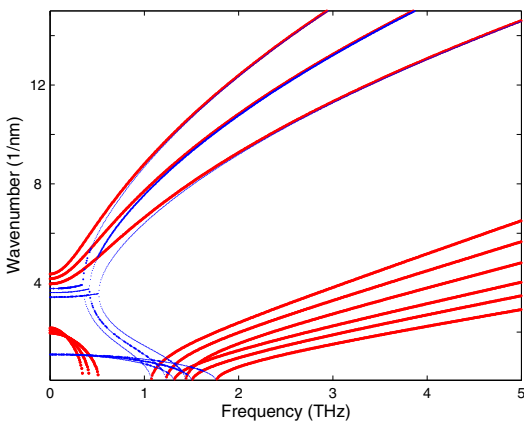
Finally, the axial wavenumbers corresponding to a fixed circumferential wavenumber $k_s R = 1$ are plotted in Figs. 6(a), (b) and (c) for single, double and three-walled carbon nanotubes respectively. The trend is quite similar to the wavenumbers in circumferential direction presented in all the previous examples. The axial mode shows a non-linear variation with the frequency. The circumferential wave mode propagates after a certain cut-off frequency. This cut-off frequency increases from the inner to the outer walls. For the radial mode, there is a cut-off frequency band within which the corresponding wave does not propagate. This is in congruence with that observed for the wavenumbers in circumferential direction, shown in the previous examples.

4 Conclusions

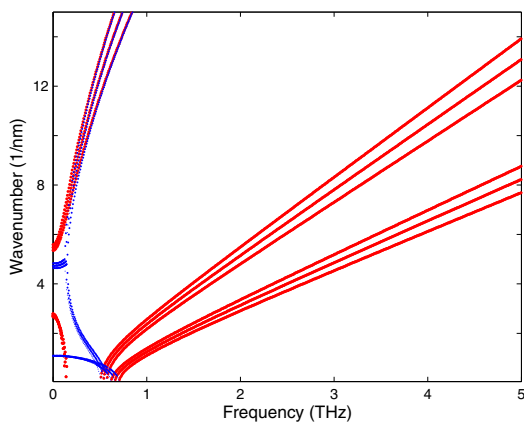
In this paper, wave characteristics of multi-walled carbon nanotubes are studied by modeling them as multiple thin shells coupled through van der Waals force. The modeling is done based on Flügge's shell theory, with each wall having axial, circumferential and radial degrees of freedom. The wavenumbers are obtained by transforming the governing wave equations to frequency and wavenumber domain through FFT. The transformed ODEs are solved by posing them as polynomial eigenvalue problem. Numerical examples are presented to study the wavenumber, phase speed and group speed of an infinite length MWNT, *i.e.*, without any variation along the axial direction. For such case, the axial wave mode is non-dispersive while the other two modes are dispersive in nature. In addition, the ax-



(a)

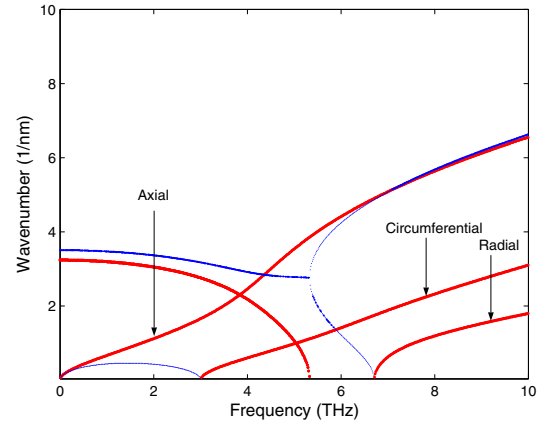


(b)

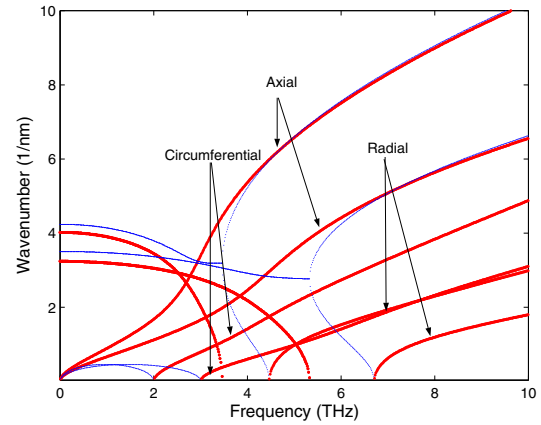


(c)

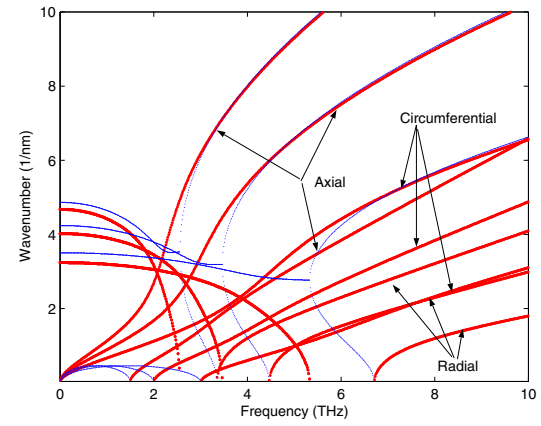
Figure 5: Real (thick line) and imaginary (thin line) parts of the wavenumbers of three walled carbon nanotubes at axial wavenumber $k_z R = 1$ for (a) $R = 1$ nm, (b) $R = 2$ nm and (c) $R = 5$ nm.



(a)



(b)



(c)

Figure 6: Real (thick line) and imaginary (thin line) parts of the axial wavenumbers of (a) single, (b) double and (c) three walled carbon nanotubes.

ial and radial wave modes do not have any cut-off frequency, but the radial mode has a cut-off frequency band within which it does not propagate. Next, wavenumbers are calculated for finite length MWNT, where, the three modes are coupled due to the finiteness of the MWNT. Here, all the modes are dispersive. The circumferential mode has a cut-off frequency and this decrease from the inner wall to the outer wall. On the other hand, the radial mode shows a cut-off frequency band within which the wave do not propagate. Another important conclusion that can be drawn from the analysis is that for MWNTs with the innermost radius higher than a certain value, the wave characteristics of each of the walls nearly coincide. Thus, in such case, the MWNT can be modeled considering an equivalent single wall instead of the multiple walls. This is in congruence with that observed for the spectrum relation of MWNT modeled as multiple Euler-Bernoulli beam coupled through van der Waals force.

References

- Chakraborty, A.; Gopalakrishnan, S.** (2005): A spectrally formulated plate element for wave propagation analysis in anisotropic material. *Computer Methods in Applied Mechanics and Engineering*, vol. 194, pp. 4425–4446.
- Chakraborty, A.; Gopalakrishnan, S.** (2006): Spectral element based model for wave propagation analysis in multi-wall carbon nanotubes. *International Journal of Solids and Structures*, vol. 43, pp. 279–294.
- Chakraborty, A.; Sivakumar, M. S.; Gopalakrishnan, S.** (2006): Spectral element based model for wave propagation analysis in multi-wall carbon nanotubes. *International Journal of Solids and Structures*, vol. 43, pp. 279–294.
- Chico, L.; Pérez-Álvarez, R.** (2004): Continuum model for long-wavelength optical phonons in cylinders: Application to carbon nanotubes. *Physical Review B*, vol. 69, pp. 035419.
- Dresselhaus, M. S.; Eklund, P. C.** (2000): Phonons in carbon nanotubes. *Advances in Physics*, vol. 49, pp. 705–814.
- Jiang, H.; Lu, J.; Yu, M. F.; Huang, Y.** (2008): Carbon nanotube transmission between linear and rotational motions. *CMES: Computer Modeling in Engineering and Sciences.*, vol. 24, pp. 95–102.
- Markus, S.** (1988): The mechanics of vibration of cylindrical shells. Elsevier, Amsterdam.
- Mitra, M.; Gopalakrishnan, S.** (2006): Wave propagation analysis in carbon nanotube embedded composite using wavelet based spectral finite elements. *Smart Materials and Structures*, vol. 15, pp. 104–122.
- Mitra, M.; Gopalakrishnan, S.** (2007): Vibrational characteristics of single-walled carbon nanotube: Time and frequency domain analysis. *Journal of Applied Physics*, vol. 101, pp. 114320.
- Natsuki, T.; Endo, M.; Tsuda, H.** (2006): Vibration analysis of embedded carbon nanotubes using wave propagation approach. *Journal of Applied Physics*, vol. 99, pp. 034311.
- Natsuki, T.; Endo, M.; Tsuda, H.** (2007): Wave propagation in single and double-walled carbon nanotubes filled with fluid. *Journal of Applied Physics*, vol. 101, pp. 034319.
- Park, J. Y.; Cho, Y. S.; Kim, S. Y.; Jun, S.; Im, S.** (2006): A quasicontinuum method for deformation of carbon nanotubes. *CMES: Computer Modeling in Engineering and Sciences.*, vol. 11, pp. 61–72.
- Raichura, A.; Dutta, M.; Strocio, M. A.** (2003): Quantized acoustic vibrations of single-wall carbon nanotube. *Journal of Applied Physics*, vol. 94, pp. 4060.
- Saito, R.; Takeya, T.; Kimura, T.; Dresselhaus, G.; Dresselhaus, M. S.** (1998): Raman intensity of single-walled carbon nanotubes. *Physical Review B.*, vol. 57, pp. 4145.
- Srivastava, D.; Wei, C.; Cho, K.** (2003): Nanomechanics of carbon nanotubes and composites. *ASME Trans. Applied Mechanics Review*, vol. 56, no. 2, pp. 215–230.

- Sun, C.; Liu, K.** (2007): Vibration of multi-walled carbon nanotubes with initial axial loading. *Solid State Communications*, vol. 143, pp. 202–207.
- Suzuura, H.; Ando, T.** (2002): Phonons and electron-phonon scattering in carbon nanotubes. *Physical Review B*, vol. 65, pp. 235412.
- Theodosiou, T. C.; Saravanos, D. A.** (2007): Molecular mechanics based finite element for carbon nanotube modeling. *CMES: Computer Modeling in Engineering and Sciences.*, vol. 19, pp. 121–134.
- Wang, C. Y.; Ru, C. Q.; Mioduchowski, A.** (2004): Applicability and limitations of simplified elastic shell equations for carbon nanotubes. *Journal of Applied Mechanics.*, vol. 71, pp. 622.
- Wang, C. Y.; Ru, C. Q.; Mioduchowski, A.** (2004): Applicability and limitations of simplified elastic shell equations for carbon nanotubes. *Journal of Applied Mechanics*, vol. 71, pp. 622–631.
- Wang, C. Y.; Ru, C. Q.; Mioduchowski, A.** (2005): Axisymmetric and beamlike vibrations of multiwall carbon nanotubes. *Physical Review B*, vol. 72, pp. 075414.
- Wang, C. Y.; Ru, C. Q.; Mioduchowski, A.** (2005): Vibration of multiwall carbon nanotubes. *Journal of Applied Physics*, vol. 97, pp. 114323.
- Xie, G. Q.; Han, X.; Long, S. Y.** (2007): Characteristics of waves in multi-walled carbon nanotubes. *Computers, Materials and Continua.*, vol. 6, pp. 1–12.
- Xie, G. Q.; Long, S. Y.** (2006): Elastic vibration behaviors of carbon nanotubes based on micropolar mechanics. *Computers, Materials and Continua.*, vol. 4, pp. 11–20.
- Yakobsen, B. I.; Brabec, C. J.; Bernholc, J.** (1996): Nanomechanics of carbon tubes: instabilities beyond linear response. *Physical Review Letters*, vol. 76, pp. 2511.
- Yoon, J.; Ru, C. Q.; Mioduchowski, A.** (2003): Sound wave propagation in multiwall carbon nanotubes. *Journal of Applied Physics*, vol. 93, pp. 87–93.
- Yoon, J.; Ru, C. Q.; Mioduchowski, A.** (2003): Vibration of an embedded carbon nanotube. *Composite Science and Technology*, vol. 63, pp. 1533–1542.
- Yoon, J.; Ru, C. Q.; Mioduchowski, A.** (2004): Timoshenko-beam effects on transverse wave propagation in carbon nanotubes. *Composites Part B*, vol. 35, pp. 87–93.